water

MDPI

Article

Comparative Study on Scour Protection Methods for Pile Group Foundations Under Wave–Current Coupling

Bowen Weng * and Junliang Lu

Institute of Bridge Engineering, Zhejiang University of Technology, Hangzhou 310023, China
* Correspondence: wengbow@zjut.edu.cn

Abstract

Wave–current coupling significantly increases the vulnerability of underwater pile foundations to scour, making effective protection measures essential for waterborne structures. In this study, a group pile of a sea-crossing bridge in Zhejiang province, China, was selected as the research object, and fifteen scour simulations were conducted using FLOW-3D v11.2 to investigate the effects of water depth, flow velocity, and wave action on the scour characteristics of pile groups. Furthermore, the performance of two protection strategies (riprap and sacrificial piles) was comparatively analyzed. The results showed that the presence of waves altered the scour pattern, while variations in water depth influenced the scour morphology through changes in the downflow structure. Under wave–current coupling, variations in flow velocity affected the distribution of the scour depth profile. Without protection, the maximum scour occurred between the second and third rows of upstream piles, with an average scour depth exceeding 7 m. When protection measures were applied, square riprap exhibited a superior performance compared to elliptical riprap. A 2 m thick square riprap layer effectively reduced the maximum scour depth by 89%. Sacrificial piles alone provided limited protection, reducing the maximum scour depth by 25%. These findings provide valuable insights for optimizing scour protection design under complex wave–current conditions.

Keywords: pile foundation; local scour; wave–current coupling; FLOW-3D simulation; riprap protection; sacrificial piles

Academic Editor: Chin H Wu

Received: 9 November 2025
Revised: 27 November 2025
Accepted: 2 December 2025
Published: 5 December 2025

Citation: Weng, B.; Lu, J. Comparative Study on Scour Protection Methods for Pile Group Foundations Under Wave–Current Coupling. *Water* **2025**, *17*, 3457. https://doi.org/10.3390/w17243457

Copyright: © 2025 by the authors. Licensee MDPI, Basel, Switzerland. This article is an open access article distributed under the terms and conditions of the Creative Commons Attribution (CC BY) license (https://creativecommons.org/licenses/by/4.0/).

1. Introduction

As a risk that affects the stability of pile foundations, scour can seriously impact the safety of water structures [1–4]. Scour around bridge piers can cause loss of supporting soil, significantly reducing the lateral support of the bridge and potentially causing the bridge to collapse without warning [5,6]. The risk of bridge failure is greatly increased when coupled with factors such as earthquakes and ship collisions. According to existing research statistics, among the many factors that cause bridge disasters, local scouring of the riverbed around the bridge foundation is generally recognized as one of the important causes of bridge failure [7,8]. Extreme weather events caused by global climate change have made it worse. Argyroudis [9] considered the potential changes in water flow (including the impact of climate change) and estimated that the scouring of 4200 railway bridges and 8700 major road bridges across waterways in the UK would increase by more than 8%. Richardson and Davis [10] also pointed the following out in a 2001 scouring research report: The United States has a large number of bridges, 86% of which are wading bridges, but more than 26,000 of them are facing or have been threatened by scouring disasters. At the

same time, sea-crossing bridges often cross vast sea areas, and the underwater environment of their foundations is more complex [11]. Tidal currents and storm surges will aggravate the impact of scouring. Within a single tidal cycle, scour and sedimentation around bridge pile foundations can fluctuate by several meters, seriously compromising the load-bearing capacity of the pile foundation [12,13]. Therefore, sea-crossing bridges are in great need of necessary scouring protection methods.

Research on the scour mechanism under wave–current coupling is an important prerequisite for studying how to provide effective scouring protection methods for pile group structures [14,15]. Many researchers have conducted extensive studies on unidirectional scouring. However, in marine environments, the rise and fall of tides create strong flood and ebb currents along the coast, with their impact being even more pronounced in estuaries [16]. Frequently changing wind directions and pressure fluctuations also affect tidal currents, making the scouring of foundations of offshore structures such as wind power platforms and sea-crossing bridges extremely complex. In extreme marine environments such as typhoons and storm surges, the depth of foundation scouring can increase dramatically, seriously threatening the structural safety of bridges [17]. Sumer et al. [18] conducted a flue test on a group of vertical piles under wave conditions and found that the scouring around the piles under wave conditions was controlled by wake vortices and horseshoe vortices. The *KC* number is the main influencing parameter of the equilibrium scouring depth under moving bed scouring conditions. Liu et al. [19] proposed a new Openfoam solver (TideflowFOAM). This solver can effectively simulate complex flow conditions under tidal flow, extending modeling capabilities to more realistic 3D bridge scouring scenarios under the combined action of waves and water flow. Kumar and Afzal [20] described the effects of relative velocity, *KC* number, absolute Reynolds number, and sediment properties on pier scour under wave–current coupling conditions. Based on statistical analysis of existing prediction formulas, they presented a calculation procedure related to scour in coastal environments under combined wave and current conditions. Although researchers have conducted extensive studies on scouring under wave–current coupling, further in-depth research is needed on the scouring mechanism of pile groups, and the influence of more key scouring parameters on scouring should be discussed.

Scouring around pile foundations is the result of the interaction between water flow, the pile body, and sediment. Based on this, after decades of research, two methods for mitigating scouring have been developed [21–23]. One is active protection, which aims to reduce the intensity of eddies around the pile foundation. Active protection mainly involves the installation of sacrificial piles. Sacrificial piles can change the direction of water flow, creating a low-velocity zone, thereby reducing the scouring depth by about 40% [24,25]. However, the effectiveness of these active protection methods can be significantly reduced or even fail when the direction of water flow and seabed topography change.

Another approach is passive protection, which involves improving the seabed's resistance to erosion to reduce erosion. Numerous studies have shown that riprap revetment is one of the most commonly used forms of foundation protection for cross-sea bridges in practical engineering [26,27]. The erosion protection mechanism of riprap revetment includes reducing downflow and horseshoe eddies; in addition, the main characteristics of riprap revetment are that the material is easy to process, the construction process is simple, and the operation is flexible [27]. Khademghaeiny et al. [28] showed that the scouring depth of prismatic boulders is weaker than that of circular boulders, and that prismatic boulders have a larger contact surface and greater stability. Wang et al. [29] conducted physical experiments to study four types of scour protection measures, including riprap. The results showed that riprap, as a passive scour protection measure, has a good protective effect. However, current research on riprap protection often focuses on river bridges. In

marine environments, the protective effect of riprap is the result of multiple factors, such as the thickness and shape of the rock, which require further research.

In summary, current research on riprap protection of pile groups under wave–current action is relatively limited. To address the shortcomings in research on pile group scour protection under wave–current coupling, this paper investigates the effectiveness of scour protection methods under wave–current coupling through numerical simulation, focusing on the scour problem of the pile foundation of a cross-sea bridge in Zhejiang Province, China. It uses FLOW-3D numerical simulation software to study the scour mechanism of pile groups under wave–current coupling through 15 sets of numerical simulations. Numerical simulation was used to compare and select the scour protection methods for pile group foundations under wave–current coupling for the first time. The influence of key scour parameters on pile group scour was analyzed from three perspectives: wave action, water depth, and flow velocity. The effects of riprap geometry, riprap thickness, and sacrificial piles on the scour protection effect were also investigated. This provides research support and technical guidance for effective scour protection of marine infrastructure.

2. Methodology

This investigation addresses the complex environment of a sea-crossing bridge under wave–current coupling. Based on numerical simulation, it explores the local scour of pile groups under different flow conditions and analyzes the effectiveness of riprap revetment and sacrificial pile arrangement in protecting against pile group scour. Therefore, this section first introduces the numerical simulation model.

2.1. Numerical Simulation

2.1.1. Governing Equations

The numerical simulation used the computational fluid dynamics software FLOW-3D to model the pile group structure and riverbed. This software is suitable for numerical modeling of wave hydrodynamics and sediment transport. The application of the submerged boundary method effectively improves the computational efficiency of the numerical simulation. The following describes the models used in the numerical modeling process:

Fluid flushing calculations involve solving partial differential equations. With the development of methods for solving partial differential equations, the VOF method, which simulates the free surface changes of liquids, has begun to be applied to numerical simulation research. Based on FLOW-3D, this paper uses the multiphase flow continuity equation (mass conservation equation), the Reynolds-averaged Navier–Stokes equations (momentum equation), and the RNG k-ω turbulence model. In a Cartesian coordinate syst~em, the VOF model and the Euler model are employed to improve the model's computational accuracy and solution speed. The main governing equations are referenced [30] as follows:

$$\partial u_i / \partial x_i = 0 \tag{1}$$

$$\partial u_i / \partial t + u_j \partial u_i / \partial x_j = -\partial p / \rho \partial x_j + \partial [(v + v_t)(\partial u_i / \partial x_j + \partial u_j / \partial x_i)] / \partial x_j + g_i \tag{2}$$

where the subscripts i and j are 1 and 2 for the horizontal and vertical components, respectively; u_i is the fluid velocity (m/s); ρ is the fluid density (kg/m^3); p is the fluid pressure; v is the fluid dynamic viscosity (N·s/m^2); v_t is the eddy viscosity; and t is the time.

This paper selects the RNG k-ω turbulence model to solve turbulence. The reason for selecting the RNG k-ω turbulence model is that the model has a good comprehensive performance in terms of computational efficiency and accuracy [31]. It can reduce the computational time while ensuring the accuracy of the solution. The model expression is as follows:

$$\partial k/\partial t + u_j \partial k/\partial x_j = \partial\left[(\nu + \nu_t/\sigma_k) + \partial k/\partial x_j\right]/\partial x_j + P_k - \beta_k k\omega \quad (3)$$

$$\partial \omega/\partial t + u_j \partial \omega/\partial x_j = \partial\left[(\nu + \nu_t/\sigma_\omega) + \partial \omega/\partial x_j\right]/\partial x_j + \omega\alpha P_k/k - \beta_k \omega^2 \quad (4)$$

where ω is the specific dissipation rate; k is the turbulent kinetic energy; P_k is the turbulence generation rate, and the values of other coefficients are $\alpha = 5/9$, $\beta_k = 9/100$, $\beta = 3/40$, $\sigma_k = 2$, $\sigma_\omega = 2$.

2.1.2. Sediment Transport Model

The sediment model in FLOW-3D software can calculate sediment transport processes, mainly including bedload transport and suspended sediment transport. Bedload transport refers to the phenomenon where the initial velocity of sediment on the riverbed exceeds the critical velocity, causing sediment particles to roll, jump, and slide along the riverbed surface. Suspended sediment transport refers to the phenomenon where the shear stress on the riverbed is greater than the initial flow velocity of the sediment, causing the sediment to be suspended and move with the water flow. Under the combined action of gravity and friction, the suspended particles are deposited.

The dimensionless expression of bed shear stress is as follows [32]:

$$\tau^* = \tau/(\rho_s - \rho)gd_{50} \quad (5)$$

$$\tau^*_{c,i} = \tau_{c,i}/(\rho_s - \rho)gd_{50} \quad (6)$$

where ρ_s is the sediment density (kg/m^3); d_{50} is the sediment grain size (mm); τ is the local riverbed shear stress; τ^* is the dimensionless shear stress; and $\tau_{c,i}{}^*$ is the dimensionless critical shear stress.

The transport equations for sediment and suspended sediment adopt the Van-Rijn formula. The van Rijn model has good physical meaning, closely matches the real riverbed, and has been verified on a large scale in engineering and numerical simulations. It is still a commonly used sediment transport model in numerical simulations [33–35]. The equation for mass transport is expressed as [32]:

$$q_{b,i} d_i^{3/2}/\sqrt{(\rho_s - \rho)g/\rho_s} = 0.053(\tau/\tau_{c,i} - 1)^{2.1}/\left(d_{50}.\left((\rho_s/\rho - 1).g/\nu^2\right)^{0.33}\right)^{0.3} \quad (7)$$

where $q_{b,i}$ is the transport rate of bedload per unit volume; $\tau_{c,i}$ is the dimensionless critical shear stress, which can be expressed as:

$$\tau_{c,i} = (\rho_s - \rho)gd_{50}\theta_{cr} \quad (8)$$

where θ_{cr} is critical Shield number. In numerical simulations, the critical Shield number θ_{cr} is an important indicator for judging changes in the state of sediment movement. When the Shield number of sediment exceeds the critical Shield number, the sediment reaches the starting flow velocity. In this paper, the critical Shield number is obtained through the computational model proposed by Soulsby et al. [36]:

$$D_* = \left[g(s-1)/\nu^2\right]^{1/3} d_{50} \quad (9)$$

$$\theta_{\mathrm{cr}} = 0.30/1 + 1.2D_* + 0.055[1 - \exp(-0.020D_*)] \quad (10)$$

where D_* is the dimensionless diameter; s is the specific gravity of the sediment, taken as 2.65; and ν is the viscosity coefficient of water, taken as 10^{-6} m^2/s. In this paper, based

on Equations (9) and (10), and combined with the median particle size of sediment, the sediment scour parameter θ_{cr} obtained after multiple runs and calibrations is 0.044.

The transport equation for suspended mass is expressed as:

$$\partial c/\partial t + u_j \partial c/\partial x_j + w_s \partial c/\partial z = \partial\left(\Gamma \partial c/\partial x_j\right)/\partial x_j \quad (11)$$

where c is the suspended mass load concentration, which is defined as the mass of sediment per unit volume of fluid-sediment mixture; w_S is the settling velocity of sediment particles; and Γ is the value of eddy viscosity.

2.2. Test Condition Setting

Figure 1a shows the plan layout of the pile group structure for a sea-crossing bridge on the southeastern coast of Zhejiang Province. The center of the pile group coincides with the center of the foundation. The abutment measures 40 m × 40 m × 3 m. The base of the abutment is 11 m from the bed surface. The diameter of single pile is 2.5 m. There are 45 piles in total. Figure 1b shows the naming rules for each pile. From top to bottom, the rows are H1–H7, and from left to right, they are L1–L7. Therefore, H4L2 in the figure refers to the piles in the second column of the fourth row. According to related research [37,38], the extreme high tide level with a 100-year return period is 5.83 m, 1.17 m from the bottom of the abutment. The diameter of a single pile in the pile group structure above the riverbed is 2.5 m (including casing) and the pile length is 11 m. This pile group foundation is located in the Jiao River, a high-tidal estuary with irregular semi-diurnal tides. According to the tidal level data of Haimen Station from 1959 to 2016 [38], the design tidal level of the extreme high tide level with a return period of 100 years is 5.83 m, the tidal range is 6.61 m, and the flow velocity (vertical average) with a return period of 100 years is 2.35 m/s (ebb tide). The flow velocity in the waters near the group pile is relatively large, and the ebb tide velocity is greater than the flood tide velocity. It is a strong tide area, and the strong tide effect caused by the tide is obvious. The group pile in the area is mainly affected by the ENE–SE outward sea waves. The maximum wave height can reach 5.29 m, corresponding to a wave period of 15.9 s and a wavelength of 164.4 m, thereby reflecting both typicality and representativeness of strong-tidal coastal conditions.

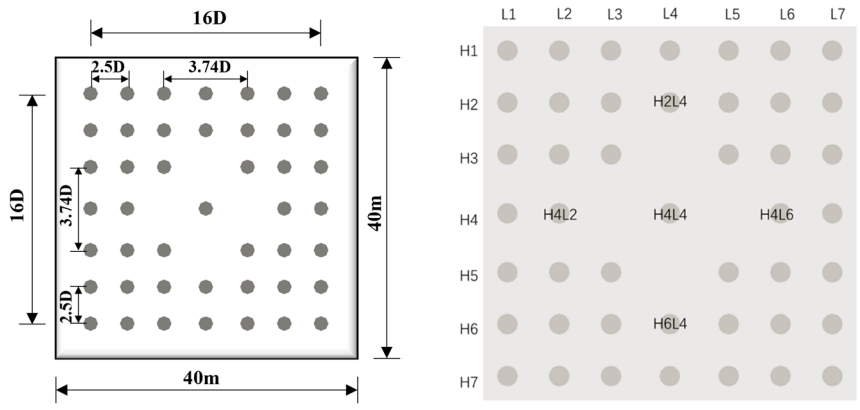

(**a**) Foundation platform pile layout (**b**) Naming rules for each pile

Figure 1. Schematic diagram of pile group structure.

To further investigate the local scouring patterns around the pile foundations under tidal currents, the hydrological conditions in the region under different return periods were statistically analyzed, as shown in Table 1, which includes high tide and low tide levels.

Table 1. Tidal current statistical conditions.

Return Period	Velocity/(m/s)	Water Depth (High and Low)/m	Wave Height (High and Low)/m	Cycle/s	Wavelength (High and Low)/m
(1) 100-year	2.35	9.83/1.09	5.29/0.64	15.9	164.4/77.4
(2) 50-year	2.15	9.48/1.2	5.06/0.66	15.1	151.4/75.7

The sand-bed in the area is mainly composed of silt (plastic state), silty clay (mainly distributed in the riverbed section, with a relatively thick thickness), clay and round gravel soil. The water flow and sediment conditions are complex, and the scouring and sedimentation conditions are complex and changeable. As shown in Table 2, the sediment parameters used in this investigation refer to the mathematical statistics table of physical and mechanical indicators of foundation soil provided by the latest relevant research data [39]. According to the results of the bottom sediment sampling in the area, the bottom sediment particle size at the group pile is small and has a strong anti-scouring ability. Scouring mainly occurs in (1) silt and (2) silty clay, and there is cohesion between particles. In numerical simulation studies, the median particle size of sediment is an important parameter for calculating sediment transport. However, in the geological survey of the engineering example, the median particle size of the sediment at the bottom of the group pile was not directly given. As can be seen from the research of Chien and Wan [40], the cohesion of cohesive soil makes it more difficult for sediment to be initiated. Based on the results of the initiation velocity test of cohesive soil, Mao et al. [41] and Zhou [42] calculated the equivalent particle size by back-calculating the initiation velocity formula. The relevant results have been verified by a lot of experimental data and actual scouring of the downstream channel of the sluice gate in Jiangsu Province, China [42,43]. Future research will combine physical experiments to collect actual sediment samples from the study area, analyze the sediment moisture content and cohesive soil content, and conduct research on pile scour. In this paper, considering the safety and durability of the project, the cohesion of the silt in the group pile layer (1) is taken as 8 kPa as the reference parameter. The equivalent particle size equation of non-cohesive sand in numerical simulation is used as follows [40]:

$$D_{50} = 0.34(c/10g)^{2.5} \tag{12}$$

where c is the interparticle cohesion, taken as 8 kPa based on sampling results; D_{50} is the impact-equivalent particle size (m). Calculations show that the sediment particle size selected for this investigation is 0.65 mm.

Table 2. Physical and mechanical indicators of soil.

	Water Content/%	ρ g/cm^3	Proportion	Cohesion/kPa
(1) silt	60.2	1.63	2.65	8
(2) silty clay	46.5	1.74	2.72	12

Different countries refer to different calculation models when selecting the riprap particle size during the design phase. In Appendix D3.4 of GB 50286-2013 (China) [44], the calculation equation for the stable impact-resistant particle size (converted particle size) of the protective engineering block stone is:

$$d = V^2\gamma/2C^2g(\gamma_s - \gamma) \tag{13}$$

$$W = \pi d^3\gamma_s/6 \tag{14}$$

where d is the converted particle size of the riprap; W is the weight of the rock; V is the velocity of the approaching flow; g is the acceleration of gravity; γ_s is the specific gravity of the riprap; C is the stability coefficient of the rock movement, which is 1.2.

In the above equation, the stone blocks are converted into the diameter of a sphere. In addition to the water velocity, the stone block density and low slope conditions are also considered. However, this specification does not directly consider the impact of bridge piers.

According to the US HEC-18 report [45], the equation for calculating the particle size of riprap is:

$$d = 0.692(KV)^2/2(S_s - 1)g \quad (15)$$

where K is the pile shape factor, which is taken as 1.5; S_s is the specific gravity of the riprap, which is taken as 2.65. In this study, in order to fully ensure the stability of the riprap, the larger value of Equations (13) and (15) was selected as the calculated value of the riprap size.

In this investigation, the comparison of riprap and sacrificial piles as scour protection methods is mainly considered. At the same time, factors such as different riprap layer geometries, riprap layer thicknesses, and different pile spacing ratio (L/D) are taken into consideration. The pile spacing ratio is the ratio of the distance between the center of the sacrificial pile and the single pile to the diameter of the single pile. The applicability of the protection methods is evaluated through numerical simulations.

The Keulegan–Carpenter number (KC number) is a dimensionless parameter representing the proportion of the net horizontal distance traveled by a wave within one cycle to the structural scale. A larger KC number indicates a more complex flow regime. In studies of bridges, pile foundations, and underwater structures, KC is a key indicator for assessing wave–current scouring, eddy shedding patterns, and bed sediment movement [46]. The KC number can be calculated using the following equation:

$$KC = U_m T/D \quad (16)$$

where U_m is the velocity near the bed surface caused by waves, T is the wave period, and D is the pile diameter.

However, due to the lack of field scour and hydrological monitoring data for this cross-sea bridge, this paper mainly refers to the hydrological survey report of the adjacent sea area and the bridge's design hydrological parameters for analysis. The study focuses on the protective effects of riprap and sacrificial piles under the most unfavorable hydrological conditions in the design. In subsequent research, the author will conduct long-term scour monitoring of the bridge and, combined with physical experiments, conduct a more in-depth study of pile group scour protection in this marine environment. Based on the above hydrological conditions, and considering the working conditions of pile group scour with or without scour protection, 15 sets of numerical simulation software (Table 3) were set up as follows:

In order to investigate the effect of protection methods on reducing the impact of pile group foundations, this paper used Flow-3D v11.2 to conduct numerical simulations. This software is capable of tracking fluid boundary layers and resolving fluid–fluid and fluid–air interfaces using rectangular non-boundary fitting coordinates. It has been widely used in coastal engineering and to study flow field structure and local scour depth evolution around bridge pile foundations [47]. The mass continuity and momentum equations for the fluid used in Flow-3D have been extensively discussed elsewhere in the literature and will not be repeated here. Detailed equations and verification of the accuracy of the scour simulation can be found in the study by Guo et al. [30].

Table 3. Numerical simulation condition settings.

Test 1. 100-Year Return Period Velocity + High Tide Level + Waves					
Wave height/m	Cycle/s	Wavelength/m	*KC* number	Water depth/m	Velocity/(m/s)
5.29	15.9	164.4	3.41	9.83	2.35
Test 2. 100-year return period velocity + low tide level + waves					
Wave height/m	Cycle/s	Wavelength/m	*KC* number	Water depth/m	Velocity/(m/s)
0.64	15.9	77.4	0.62	1.09	2.35
Test 3. 50-year return period velocity + high tide level + waves					
Wave height/m	Cycle/s	Wavelength/m	*KC* number	Water depth/m	Velocity/(m/s)
5.06	15.1	151.4	3.11	9.48	2.15
Test 4. 50-year return period velocity + low tide level + waves					
Wave height/m	Cycle/s	Wavelength/m	*KC* number	Water depth/m	Velocity/(m/s)
0.66	15.1	75.7	0.63	1.2	2.15
Test 5. 100-year return period flow velocity + 100-year return period high tide level + unidirectional flow					
Velocity/(m/s)				Water depth/m	
2.35				9.83	
Test 6. 100-year return period flow velocity + 100-year return period low tide level + unidirectional flow					
Velocity/(m/s)				Water depth/m	
2.35				1.09	
Test 7. 50-year return period flow velocity + 50-year return period high tide level + unidirectional flow					
Velocity/(m/s)				Water depth/m	
2.15				9.48	
Test 8. 50-year return period flow velocity + 50-year return period low tide level + unidirectional flow					
Velocity/(m/s)				Water depth/m	
2.15				1.20	
Local scour simulation with riprap protection					
Test 9					
Wave height/m	Wave Cycle/s	Wavelength/m	Water depth/m	Velocity/(m/s)	Riprap Shape	Size/m	Thickness/m
5.29	15.9	164.4	9.83	2.35	Square	80 × 80	1.5
Test 10							
Wave height/m	Wave Cycle/s	Wavelength/m	Water depth/m	Velocity/(m/s)	Riprap Shape	Size/m	Thickness/m
5.29	15.9	164.4	9.83	2.35	Square	80 × 80	0.8
Test 11							
Wave height/m	Wave Cycle/s	Wavelength/m	Water depth/m	Velocity/(m/s)	Riprap Shape	Size/m	Thickness/m
5.29	15.9	164.4	9.83	2.35	Ellipse	Long axis: 100 Short axis: 80	1.5
Test 12							
Wave height/m	Wave Cycle/s	Wavelength/m	Water depth/m	Velocity/(m/s)	Riprap Shape	Size/m	Thickness/m
5.29	15.9	164.4	9.83	2.35	Square	80 × 80	2
Test 13							
Wave height/m	Wave Cycle/s	Wavelength/m	Water depth/m	Velocity/(m/s)	Riprap Shape	Size/m	Thickness/m
5.29	15.9	164.4	9.83	2.35	Ellipse	Long axis: 100 Short axis: 80	2
Local scour simulation under sacrificial pile protection							
Test 14							
	Wave		Water depth/m		Velocity/(m/s)	Sacrificial pile diameter/m	*L/D*
Wave height/m	Cycle/s	Wavelength/m					
5.29	15.9	164.4	9.83		2.35	2.5	2
Test 15							
	Wave		Water depth/m		Velocity/(m/s)	Sacrificial pile diameter/m	*L/D*
Wave height/m	Cycle/s	Wavelength/m					
5.29	15.9	164.4	9.83		2.35	2.5	1.5

The model's computational domain dimensions are shown in Figure 2a. The computational domain is 180 m long and 130 m wide, with a pile group model located in the center. The pile group model dimensions refer to Figure 1a. The piles above the riverbed are 11 m long, and the riverbed thickness is set to 20 m. Figure 2b shows the model's boundary conditions. Because wave conditions were considered in this study, a wave boundary was used at the model's inlet. For flow condition settings, refer to Table 4. After setting the water depth to 9.83 m, wave conditions still needed to be defined in the software. Elliptical cosine waves were chosen for simulation, with a flow velocity of 2.35 m/s, a wave height of 5.29 m, and a period of 15.9 s. The outlet boundary was a pressure boundary, and a wave-breaking

section was set 5 m afterward to ensure smooth discharge of the fluid model and prevent backwater from forming within the calculation area under the action of waves. The ground was set as a wall condition, the top as a pressure boundary, and the remaining boundary conditions were symmetric boundaries. Figure 2c illustrates the mesh of the pile group structure. To improve numerical simulation accuracy, the mesh around the pile group was locally refined. The center of the mesh refinement zone measures 80 m × 80 m × 40 m. Within the refinement zone, the mesh is a uniform cube with a side length of 0.5 m. The mesh outside the refinement zone is a uniform cube with a side length of 1 m.

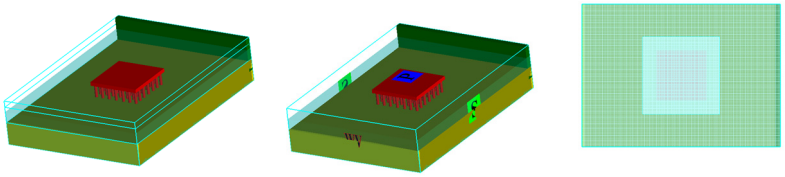

(**a**) Overall model. (**b**) Boundary condition. (**c**) Grid conditions.

Figure 2. Model layout.

Table 4. Physical parameters of the mesh verification model.

Single Pile Diameter/m	Pile Length/m	Water Depth/m	Velocity/(m/s)	Scour Depth/m
2.5	45	12	2.41	15.5

The mesh is fundamental to numerical simulation. The degree of discretization of the equations is determined by the mesh size, while the accuracy and stability of the computation depend on the mesh size. Therefore, sensitivity analysis of the mesh size is necessary. Since direct field monitoring data on the scour depth of the sea-crossing bridge studied in this paper is lacking, the nearby Taizhou Bay Bridge on the Jiao River is used as the object of the mesh sensitivity study to improve the accuracy of the research. The scour monitoring data for the Taizhou Bay Bridge comes from the research of Yun and Chen et al. [48]. Table 4 shows the pile group parameters, hydrological conditions, and maximum scour depth for the simulated working conditions. Figure 3a is a schematic diagram of the Taizhou Bay Bridge, and Figure 3b shows the mesh refinement of the pile group model. Three main mesh sizes are set: 2 m, 1 m, and 0.5 m. The mesh sizes in the intermediate refinement area are all half the main mesh sizes, i.e., 1 m, 0.5 m, and 0.25 m.

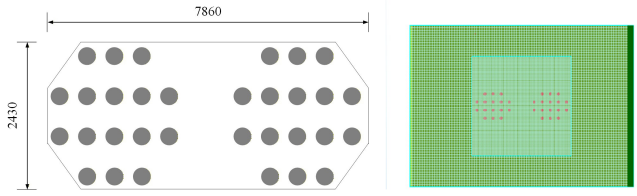

(**a**) Overall model. (**b**) Grid conditions.

Figure 3. Model layout of Taizhou Bay Bridge.

To verify the results of the numerical solution, the scour depths obtained from three different computational meshes are listed in Table 5, where d_m represents the maximum scour depth. The table shows that as the mesh size decreases, the mean error between the calculated and measured values also decreases. When the mesh size is 2 m, there is a significant difference between the calculated and measured values (i.e., 25%), which may be because the diameter of the bridge pier is 2.5 m, very close to the size of a single mesh,

resulting in a large error. When the mesh size is reduced to 1 m, the error tends to stabilize at approximately 6.7%. When the size is reduced to 0.5 m, the average error decreases by only 1.3%; however, the number of meshes increases by 20,888,000. Therefore, taking into account both error and computation time, a grid size of 1 m was determined as the optimal choice for numerical simulation.

Table 5. The sensitivity analysis of the mesh size.

Model	Main Mesh Size/m	Number of Cells	d_m/m	Mean Error/%
Field measurement	-	-	15.5	-
1	2	373,000	19.4	25.2
2	1	2,984,000	14.5	6.5
3	0.5	23,872,000	14.7	5.2

2.3. Simulation Accuracy Verification

In this paper, the comparison of the scour protection effect of the pile group structure in the water was carried out by FLOW-3D software. The accuracy of the scour morphology simulation using FLOW-3D software has been assessed in the previous single pile study [30]. According to the data in Table 5, under the test with a main mesh size of 1 m, the error between the maximum scour depth of the pile group calculated by numerical simulation and the actual field measurement data is 6.5%. Meanwhile, in the study by Daneshfaraz et al. [33], the feasibility of using FLOW-3D v11.2 for simulating pile scour was also verified through physical experiments. Comparative results showed that the relative errors in simulating different pile scour depths within the pile group were relatively small, all less than 0.5%, and the coefficients of determination were all close to 1, indicating that using FLOW-3D to simulate pile scour is acceptable. In summary, it can be found that the FLOW-3D software has good accuracy in the pile group scour simulation process.

Figure 4 shows the topographic map of the pile group scour during test 1 under balanced scour. The scour pit is generally spoon-shaped, with deeper scour on the upstream side of the pile group structure and relatively shallower scour on the downstream side. Due to the jet effect, the maximum scour location appears between the first and second rows of piles on the upstream side, located on both sides of pile H4L2. The overall scour pattern of the riverbed and the location of the maximum scour are similar to the pile group scour phenomenon observed by Yang et al. [49] in the experiment. In summary, the Flow-3D software can successfully simulate the local scour of pile groups under wave–current coupling.

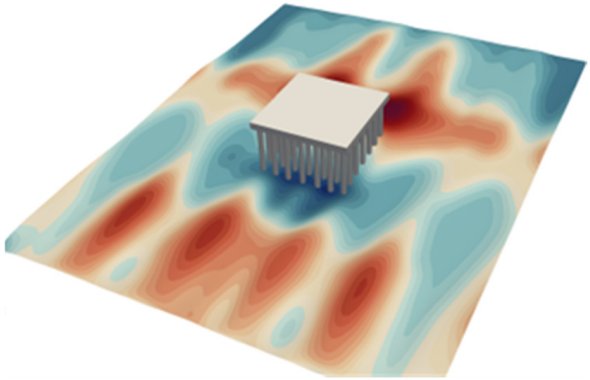

Figure 4. Scour depth contours for test 1.

3. Results and Discussion

3.1. Influence of Water Flow Conditions on Pile Scour

Local scour is caused by a complex process and is the result of the interaction between water flow, sediment and structure. It is affected by many factors. Existing research shows [32] that hydraulic factors, pile shape and arrangement factors, and sediment properties are all key factors affecting scour. Among the hydraulic factors affecting scour, flow velocity and water depth have been identified as the main parameters controlling scour. These parameters greatly affect the vortex structures around the structure, such as horseshoe vortices and wake vortices, which control local scour. When waves and water flow are superimposed, the presence of waves will also change the vortex structure of the water flow, which will have a significant impact on local scour and may amplify the local scour depth around the structure [16]. This section will analyze the influence of hydraulic factors on local scour of pile group structures.

3.1.1. The Impact of Waves on Local Scour

As shown in Figure 5a,d, the superposition of waves significantly affects the approach velocity. In Figure 5d, under test 5, the velocity distribution is uniform, with only the area around the structure experiencing disturbance, resulting in flow acceleration and vortex structures. However, in Figure 5a, the velocity and approach depth change with the propagation of the wave crest. When the wave crest passes over the pile group structure, the flow acceleration around the piles is more pronounced compared to test 5 (unidirectional flow), and there are significant velocity differences between the pile groups, exhibiting a clear jet phenomenon, which is consistent with the numerical simulation results of Yang et al. [50]. Meanwhile, unlike single-pile scouring, pile group scouring exhibits the following effects: upstream shielding effect, meaning the presence of upstream piles weakens the horseshoe vortex intensity in front of downstream piles, resulting in a greater scouring depth for upstream piles than for downstream piles; and wake vortex shedding effect, meaning that downstream piles, being within the wake vortex shedding path of upstream piles, make it easier for sediment to be suspended. In Figure 5, it can be observed in the flow field around the piles on both sides of the pile group that the rear piles are located in the wake vortex shedding area of the front piles, making it easier for sediment on the outer side of the pile group to be moved [51].

Figure 6 shows the time-varying maximum scour depth under unprotected tests. In the figure, the time for each test group was normalized (each time/equilibrium time), and the evolution of the maximum scour depth of the pile group was reflected by dimensionless time. The scour evolution curves of tests 1–4, which take into account wave–current coupling, fluctuate significantly and are sawtooth-shaped. The scour pattern is different from that of test 5. This is due to the change in flow velocity during wave propagation [52]. When the wave crest approaches, the water flow moves in the same direction as the wave. The flow velocity and flow depth reach their peak values at the wave crest position. At this time, a down flow and a horseshoe-shaped vortex are formed on the upstream side of the pile foundation. The horseshoe vortex generates a strong rotating flow at the bottom of the front side of the pile foundation, which exerts downward pressure on the bed surface on the front side of the pile foundation. The shears force on the bed surface exceeds the sediment initiation threshold, and local scour begins to develop [53]. After the wave crest passes, the flow velocity is affected by the fluid pressure. The flow velocity and flow depth reach their lowest values at the wave trough, and local scour slows down [49]. However, the water flow has a weak sand-carrying capacity at the wave trough. After passing through the pile group structure, the sediment may sink and cause local scour backfilling. Compared to unidirectional flow, the periodic action of waves causes the intensity of the

downflow in front of the pile to be inconsistent. When the downflow intensity is low, the horseshoe vortex in the scour pit is not enough to transport the sediment carried upstream to the rear. The sediment backfills in the scour pit, causing fluctuations in the scour depth [54]. This phenomenon makes the scour pattern under wave–current coupling different from that under unidirectional flow. In Figure 6, the scour evolution curve for test 5 is generally smooth, gradually approaching the equilibrium scour depth. However, when the slope angle of the scour pit exceeds the angle of repose of the sediment, the numerical simulation sand slippage algorithm corrects the sediment bed to simulate the phenomenon of sediment sliding into the scour pit. This may be the reason for the sudden changes in scour depth during the simulation. Comparing the maximum scour depths of tests 1 and 5, the maximum scour depth of test 1 was 11.45 m, while that of test 5 was 9 m. It can be found that the scour depth of the pile group under wave–current conditions is significantly greater than that under steady flow conditions, with an increase of 27.2%. This indicates that the superposition of waves can significantly enhance the scour around the piles. This is because the addition of waves increases the intensity of the eddy current, increases the shear force on the soil around the pile, and accelerates the transport rate of sediment around the pile [51].

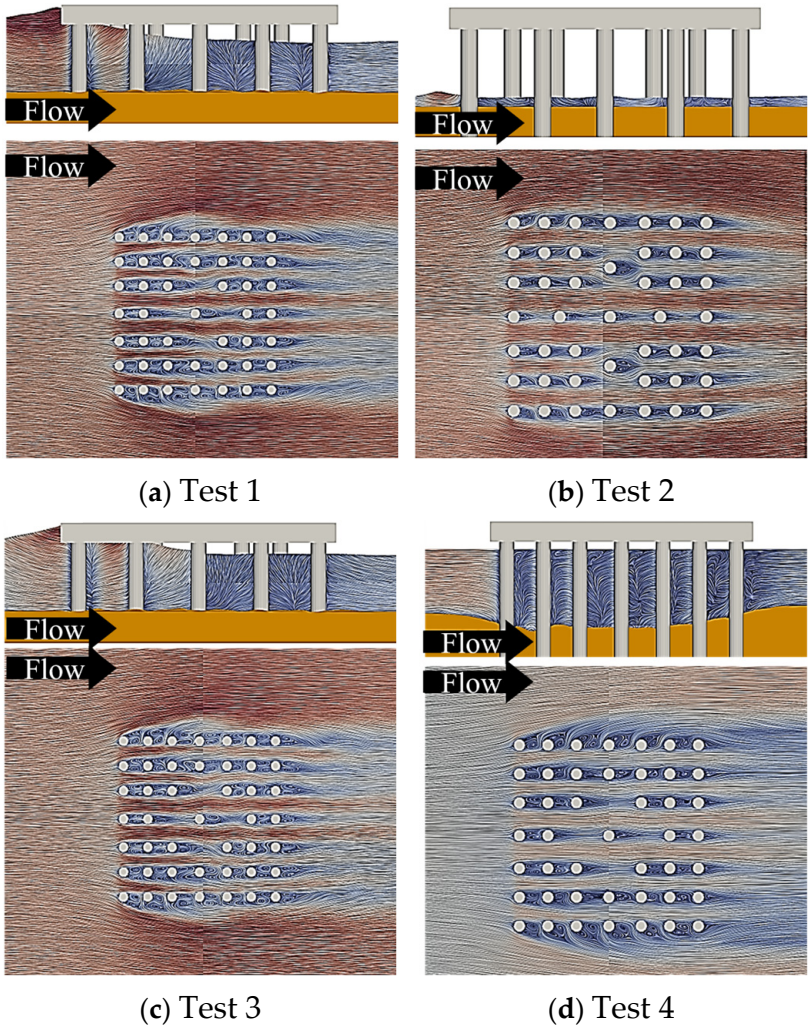

Figure 5. Streamline of unprotected test.

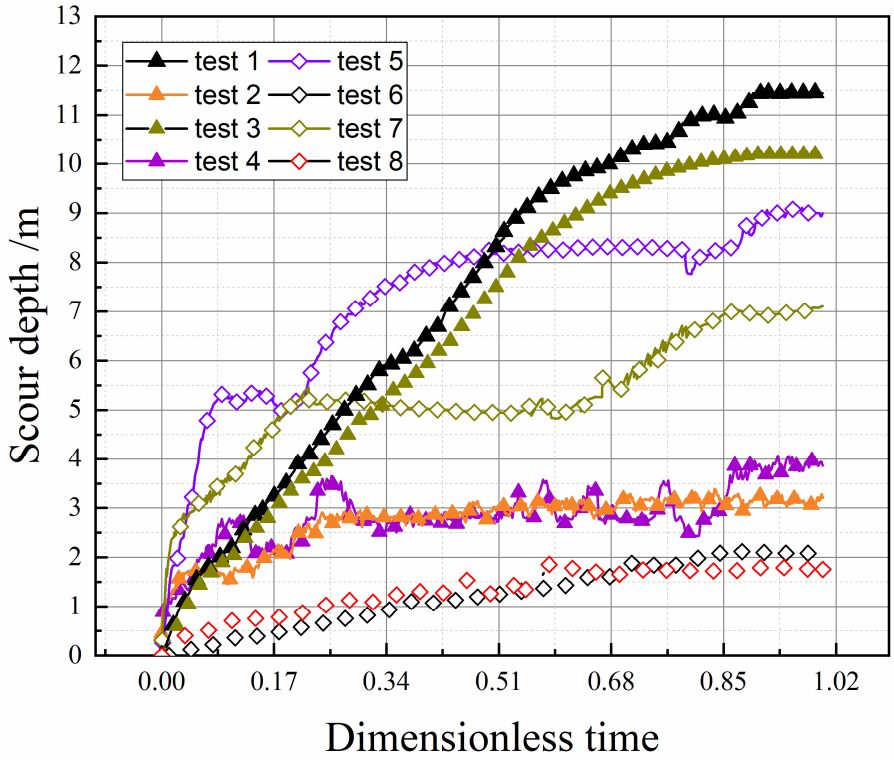

Figure 6. Maximum Scour Depth of unprotected test.

Figure 7 shows the cloud map when the scour balance is reached under the condition of no protection. Figure 8 shows the bed profile of test 1 under balanced scour. Waves also have a certain influence on the shape of the scour pit. The scour pit of test 1 is scoop shaped. The scour on the water-facing side of the pile group structure is deeper, while the scour on the rear side is relatively shallower. The maximum scour position is located between the first and second rows of piles on the water-facing side. Due to the wave–current coupling effect and the influence of the horseshoe vortex and jet between the piles, the sand-carrying capacity of the wave–current scour is increased, so that the maximum scour position appears on the pile side of the front pile. Taking the pile in the middle of the structure as the boundary, the average local scour depth of the pile group in the front half facing the water is about 10 m, and the average scour depth of the pile group in the rear half is about 7 m. The side of the pile group structure's scour depth is 9 m. Within a range of 17 m on the pile side, the scour depth is greater than 7 m. The scour range in the transverse direction is greater than that in the downstream direction, which is similar to the pile group scour morphology observed by Yang et al. [49] in the experiment. The periodic motion of waves causes the near-bed surface eddy current system to change continuously. The bed surface exhibits an undulating state under the action of waves. These wavy scouring and deposition patterns are caused by the azimuth angular velocity related to flow instability. This phenomenon occurs when eddies propagate in the water and collide with the sand bed layer. At the same time, the shedding of the wake vortex of the pile structure makes the overall scouring of the bed surface under the action of waves greater than that of steady flow [54]. In test 5, the scour pits are concentrated around the pile group structure, and the local scour range in the crossflow direction is significantly smaller than that of the wave scour. The maximum scour location is between the first and second rows of piles on the upstream side, similar to test 1. The scour depth is evenly distributed in the front and rear parts of the pile group, with an average scour depth of 7 m. Further comparison of the sand ridges between the piles in the two conditions reveals that the sand ridges between the piles become less obvious under the wave scour condition, and the accumulation height

of the sand ridges downstream of the pile group is also lower than that under the steady flow condition. This indicates that the waves enhance the scouring effect of the horseshoe vortices between the piles and also enhance the shedding of the wake vortices [16], causing sand particles to be transported downstream and reducing the accumulation behind the piles, thus explaining the above differences.

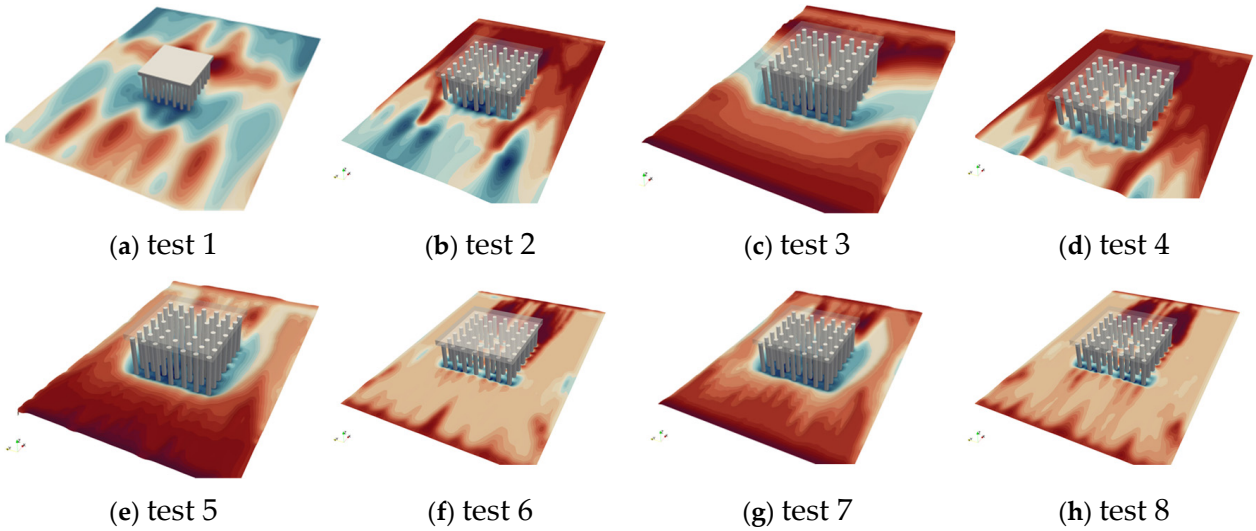

Figure 7. Group pile scour cloud map.

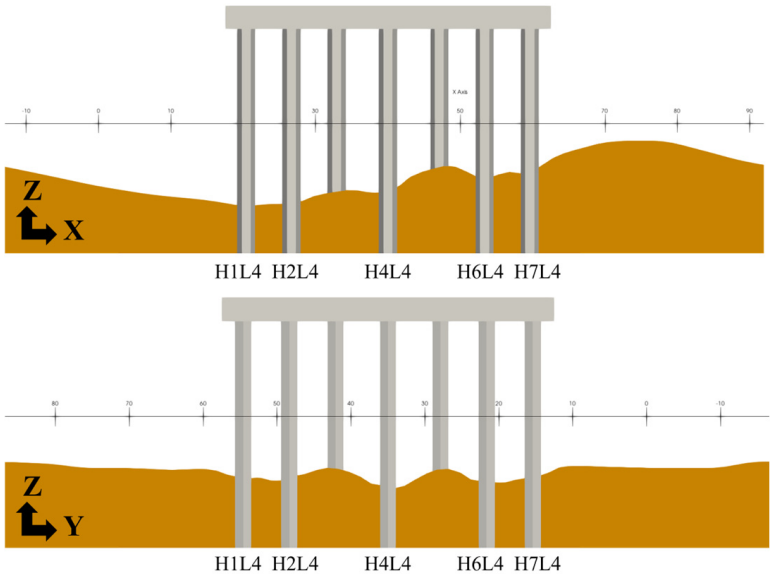

Figure 8. Profile of test 1.

3.1.2. The Effect of Water Depth on Local Scour

As shown in Figure 5a,b, test 2 represents a possible localized scour at an extreme low tide level (1.09 m). Compared to test 1, it is evident that water depth has a significant impact on localized scour. The maximum localized scour depth in test 2 is 3.3 m, a 71.2% reduction compared to test 1. Figure 5b shows that at the extreme low tide level, the downflow in front of the piles is almost invisible, while the tail vortex behind the piles is relatively small. The shallower water depth directly reduces the intensity of the downflow in front of the piles, weakening the horseshoe vortex and tail vortex, directly limiting the development of vortex structures around the pile group structure, thereby reducing the shear force on the soil around the pile and suppressing the development of localized scour. As shown

in Figure 7b, the overall scour depth of test 2 is smaller, and the maximum scour location is located between the second and third rows of piles on the upstream side. The scour pit shape is quite different from that of test 1. Local scour between piles mainly occurs in the gaps between piles. This may be because the waves are weakened by the pile group structure at low tide and cannot have a significant impact on the water flow. The water flow accelerated by the jet effect controls the scour between the pile group structure, thus forming strip-shaped scour pits between the piles. The same situation can also be seen in Figure 7d.

3.1.3. The Impact of Flow Velocity on Local Scour

As shown in Figure 7c, test 3 considers the local scour balance under a 50-year return period flow velocity (2.15 m/s). Compared with test 1, the scour pit shape is similar, and it is spoon-shaped. The scour at the rear of the pile group structure is relatively weaker than that of test 1. As can be seen in Figure 6, the reduction in flow velocity significantly reduces scour depth. At that time, the maximum scour depth of test 3 is 8.2 m, which is 3.25 m different from the maximum scour depth under extreme conditions (flow velocity 2.35 m/s) of test 1. The scour evolution curve of test 1 does not show the sawtooth development as in tests 2 and 3. This is because the water flow intensity of test 1 is higher. Even when the trough of the wave reaches the front of the pile group, the minimum flow velocity is about 1.11 m/s, while the flow velocity at the trough of the wave in test 3 is 0.61 m/s. The critical initiation velocity for sediment is 0.576 m/s, meaning that test 1 was in a live-bed scouring mode throughout. In test 3, the lowest velocity in the trough area was close to the sediment initiation velocity. Therefore, compared to Test 3, Test 1 can still maintain the scouring of the live bed even at the trough flow velocity, the effect of the downflow is obvious, the duration of the reverse pressure gradient is long, and the size, strength and life of the horseshoe vortex and wake vortex around the pile are more significant [51]. The scouring curve did not show a sawtooth shape but rather a gradual development pattern similar to unidirectional flow.

3.2. Numerical Simulation of Pile Group Scour Protection

3.2.1. The Influence of Riprap Geometry on Impact Reduction Effect

In complex tidal environments, such as sea-crossing bridges, direct riprap is a common scour prevention method, given the complexity of construction [5]. Simulations were conducted for two different riprap protection arrangements: square and elliptical, respectively, for the most unfavorable hydraulic conditions. Based on the research of Rashno et al. [55] and the engineering background, the square riprap layer dimensions were 80 m $\times$ 80 m. The elliptical arrangement ensured a similar riprap volume as the square arrangement, with a range of 100 m on the major axis, 80 m on the minor axis. Because the numerical simulation indicated that the scour range downstream of test 1 was smaller than that across the flow, the major axis was arranged across the flow.

Figure 9 shows the local scour cloud map of the pile groups with different riprap shapes, corresponding to working test 9 and 11, respectively. As can be seen in Figure 9a, local scour first occurs at the four corners of the square protective layer, and the scour pits erode into the interior of the protective layer over time. This is because, under the action of water flow, there is a phenomenon of flow acceleration at the upstream side of two sides of the riprap layer. The downflow and the accelerating flow act on the riverbed surface at the same time, which makes the sediment at this point subject to large shear stress on the riverbed surface, and it is very easy to reach the critical flow velocity of sediment. This is the same phenomenon observed by Chiew [56] in a flume experiment, that is, the riprap protective layer gradually fails from the edge, and the shape of the riprap layer causes the

greatest scour at the corners of the protective layer. Meanwhile, the riprap layer provides good protection for the bed surface inside the pile group. Downflow cannot directly act on the sand bed surface; the larger-diameter riprap effectively disperses the energy of the water flow. Since the scour pit has not developed further, the possibility of horseshoe eddies carrying sediment is further reduced. Figure 10 illustrates the local scour contour map of the pile group when the scour reaches equilibrium in tests 9 and 11. The maximum scour position is located at the corner of the square side facing the flow. In Figure 10a, the average scour depth inside the pile group structure is close to 1 m. This indicates that the riprap inside the pile group effectively protected the sand bed surface, preventing it from being directly affected by the eddy current system and scoured. Compared with the average scour depth of more than 7 m near the pile group in test 1, it can be found that the local scour inside the pile group structure is well suppressed, and the square riprap protection has a good scour protection effect. As can be summarized in Figure 11, the maximum scour depth of the bed in test 9 is 5.3 m, which is 53.7% lower than that in test 1 without protection. Riprap protection, as a passive protection method, uses larger-diameter rocks to prevent downflow, horseshoe vortex, and wake vortex systems from directly impacting the sand bed surface, thereby improving the stability of the bed surface and the safety of the structure.

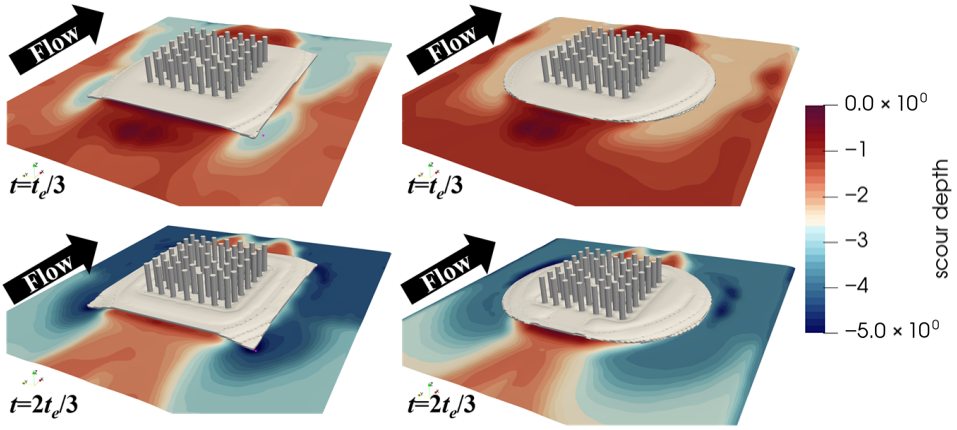

(**a**) Test 9 (**b**) Test 11

Figure 9. Local scour cloud map.

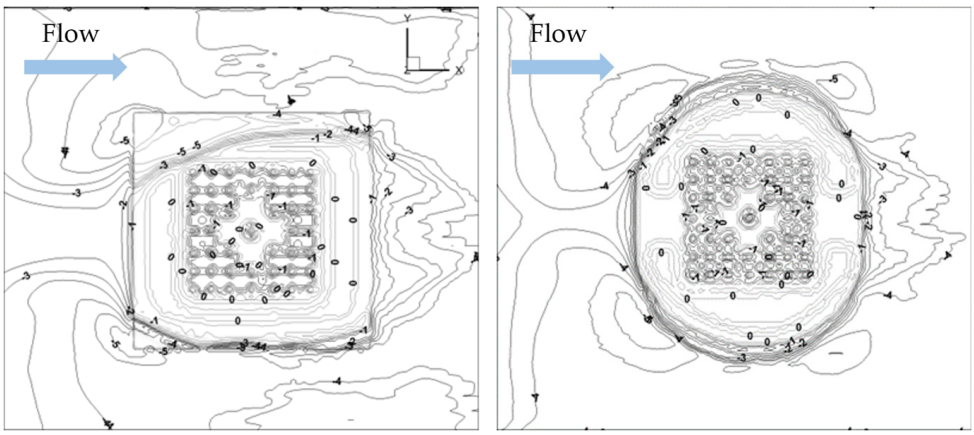

(**a**) Test 9 (**b**) Test 11

Figure 10. Equilibrium scour contour map.

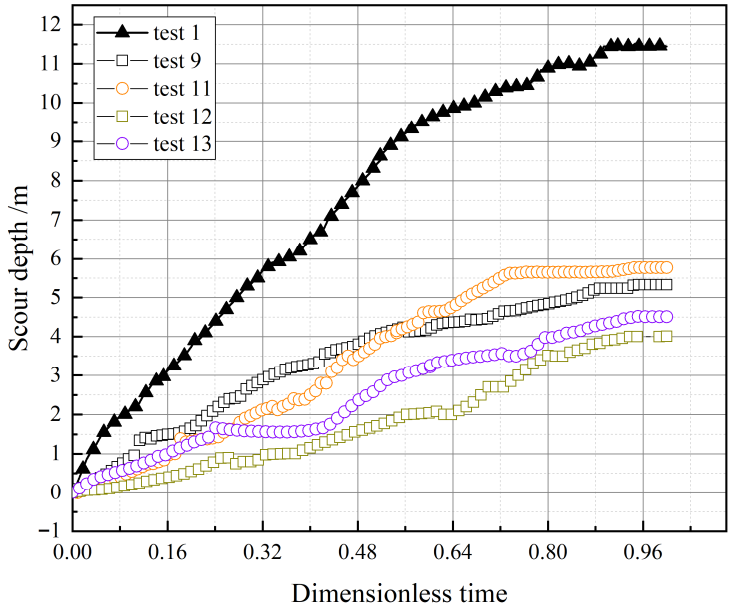

Figure 11. Evolution of the scour depth of the pile groups based on numerical simulation.

The maximum scour depth of the riverbed for test 11 is 5.8 m, located between 45° and 60° on the upstream side. The maximum scour depth under the elliptical protection is slightly deeper than that under the square protection. This is likely because the elliptical riprap structure facilitates flow acceleration around the water, leading to increased scour on the sides of the protective layer. Figure 10b shows that the average scour depth within the pile group structure under the elliptical protection is close to 1 m, which also effectively suppresses localized scour. Localized scour is primarily concentrated on the sides of the protective layer. The elliptical arrangement concentrates scour on the elliptical side where flow acceleration occurs, unlike the square arrangement, where scour is concentrated at the corners. This indicates that for riprap protection, since the riprap structure is directly set above the bed surface, the water flow effect is significant at the boundary of the riprap layer and the interface with the sand bed, and the complex eddy system causes the endpoint to be scoured first. Setting the top surface of the riprap flush with the riverbed is an effective way to reduce the scouring problem at the riprap boundary, but it is difficult to implement in practice and requires higher costs [5]. In Figure 11, comparing tests 9 and 11, and Tests 12 and 13, the maximum scour depth of the bed is lower when using square riprap than when using elliptical riprap. This indicates that geometry can also affect the protective effectiveness of riprap. In the engineering context studied here, square riprap provides better protection.

3.2.2. Effect of Riprap Thickness on Impact Reduction Effect

Figure 12 shows the variation in the maximum scour depth of a pile group with riprap thickness. Test 10, which uses three times the riprap diameter recommended by the specification. By comparing tests 9, 10, and 12, its shows that a riprap layer thickness of 2 m achieves the best internal scour reduction effect in the pile group, reaching 89%. Under wave–current conditions, a riprap layer three times the riprap diameter (0.8 m) provides poor protection, resulting in ineffective protection and a slightly smaller scour depth than unprotected conditions. However, increasing riprap thickness does not lead to an indefinite reduction in scour depth. With increasing riprap thickness (1.5 m to 2 m), the maximum scour depth changes little, indicating that, within a certain range, increasing the thickness of the riprap slope protection can effectively reduce the severity of the scour depth. Meanwhile, beyond this range, increasing the thickness of the riprap layer will

amplify the obstruction effect on water flow, resulting in more water flowing downhill and impacting the riverbed. This is not conducive to reducing the scour depth, and simply increasing the thickness of the revetment will not significantly improve the protection effect.

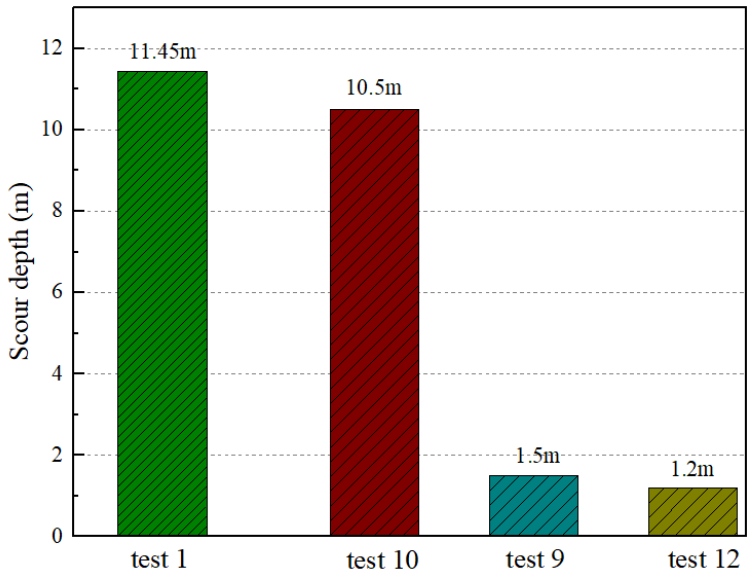

Figure 12. Effect of riprap thickness on scour protection.

3.2.3. Analysis of Protective Effect of Sacrificial Piles Under Wave–Current Coupling

In test 14, the possible scour situation under the most unfavorable water flow conditions was considered for protection. Between the sacrificial pile and the front row pile, the center distance was twice the diameter of the single pile, that is, L/D = 2, and the D of the sacrificial pile was the same as the single pile. Seven sacrificial piles were set, each located in front of the L1 row of piles on the upstream side. Figure 13 shows the change in the scour depth in the riverbed during the calculation process. The maximum scour depth was 9.2 m. According to the research of Sumer and Fredsoe [57], the scour protection effect is best when the pile spacing ratio is equal to 1.5. Therefore, test 15 considered that the center distance between the sacrificial pile and the front row pile was 1.5 times the diameter of the single pile, that is, L/D = 1.5, and the diameter of the sacrificial pile was the same as the diameter of the single pile. Figure 13 shows the changes in the scour depth in the riverbed during the calculation process. The local scour is close to equilibrium at 5600 s, and the maximum scour depth is 8.6 m. Compared with test 14, the maximum scour depth is reduced by 6.5% and the protection effect on the maximum scour depth is improved. At the same time, compared with test 1, the maximum scour depth is reduced by 24.9%, the scour protection effect of the sacrificial pile alone is limited. This may be because the sacrificial piles do not significantly weaken the water flow intensity under wave action, and the protective effect of a single sacrificial pile is limited when considering tidal action.

Figure 14 illustrates the riverbed morphology when the scour reaches equilibrium. In Figure 14a, it can be seen that at equilibrium, the scour depth of the riverbed on the upstream of the pile group is close to 6 m. Scour is more intense on the sides of the L1 row of piles and the sacrificial piles, reaching 7 m. This depth gradually decreases along the flow direction, and sediment accumulation is observed behind the pile group structure. At the same time, the maximum scour depth shifts from within the unprotected pile group to between the sacrificial piles. The maximum scour depth still occurs near the pile group, indicating limited protection compared to riprap. This is because the sacrificial piles are limited in their protective effectiveness under high flow intensities. Since the sacrificial

piles are only located on one side, they cannot effectively protect the pile group structure under tidal conditions [58].

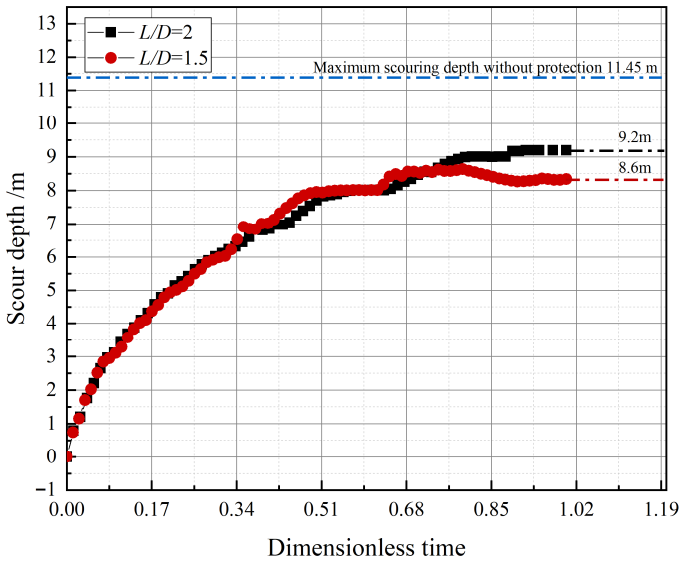

Figure 13. The scour depth development under the action of sacrificial piles (tests 14 and 15).

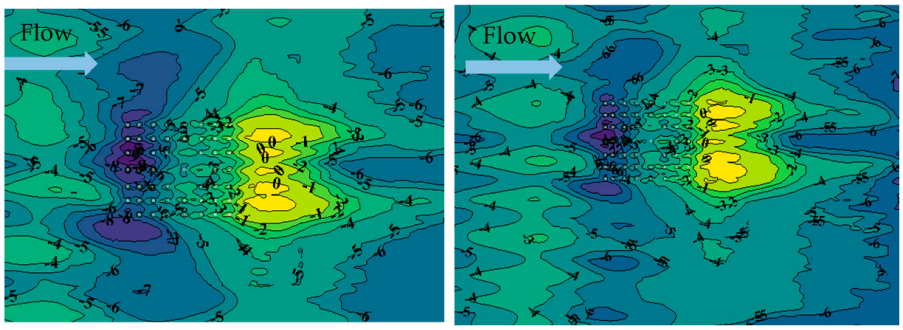

(**a**) Test 14 (**b**) Test 15

Figure 14. Riverbed scour conditions under sacrificial pile protection.

Figure 14b shows the riverbed contours when the scouring reaches equilibrium under working test 15. It can be seen that when equilibrium is reached, the riverbed scour depth on the front of the pile group approaches 5 m. Scour is more intense on the sides of the L1 row of piles and the sacrificial piles, reaching depths of 7 m. This depth gradually decreases with the flow direction, and sediment accumulation is observed behind the pile group. Compared to test 14, a smaller spacing does not significantly change the shielding effect of the pile group. Furthermore, because the sacrificial piles are closer to the upstream piles of the pile group, the scour pits of the two piles merge and develop uniformly, potentially increasing the scour depth around the sacrificial piles. Therefore, sacrificial piles are not suitable for scour protection under strong tide conditions. For this project, riprap protection is a more effective and cost-effective method.

4. Conclusions

Based on the FLOW-3D numerical simulation software, this study systematically analyzed the influence of key scour parameters on scour of the pile foundation of a cross-sea bridge in Zhejiang, China, under wave–current coupling, and investigated the scour protection effects of riprap and sacrificial pile protection, including the geometry and thickness of the riprap layer, as well as the distance between the sacrificial and protective

piles. Fifteen sets of numerical simulations of pile scour were conducted. The main conclusions are as follows: Firstly, under the model parameter settings in this paper, hydraulic conditions have a significant impact on local scour. The presence of waves alters the scour pattern. Extreme low tide levels reduce local scour and change the morphology of scour pits by affecting the downflow in front of the piles. In wave–current coupling, the relative relationship between the approach velocity and the sediment initiation velocity affects the development of scour. Secondly, according to the numerical simulation results, the geometric shape affects the scour protection effect. The square riprap layer has a better scour reduction effect than the elliptical one. The 2 m thick square protection can reduce the scour depth by 89%. The riprap layer thickness (0.8 m) with three times the riprap particle size recommended by the specification fails to provide protection under the action of wave–current coupling. After the riprap layer thickness exceeds a certain range, increasing the riprap layer thickness will not significantly enhance the scour reduction effect. Finally, when the sacrificial pile center distance L/D = 1.5, the maximum scour depth is reduced by 24.9%, indicating that the sacrificial pile has limited protection effect under the action of wave–current coupling. It can be observed that, under the hydrological conditions considered in this paper, the maximum scour depth inside the pile group under the action of riprap is less than that of the sacrificial pile, indicating that riprap protection can effectively reduce the impact of water flow on the sand bed surface and provide a better scour protection effect for the pile group structure. This approach can provide a reference for engineering projects.

This article focuses on a sea-crossing bridge in southeastern coastal China and discusses riprap and sacrificial pile protection under the most unfavorable conditions. Due to the lack of field measured scour and hydrological data, the hydrological conditions considered in this paper are limited. At high *KC* numbers (>10), different scour trends may occur, and the combined protection method of sacrificial piles and riprap is not considered. Future research will incorporate physical experiments and long-term monitoring, consider more comprehensive wave conditions, and conduct more specific studies on the design parameters of riprap protection to improve its scour-reducing effect under wave–current coupling. Simultaneously, protection methods combining riprap and sacrificial piles, as well as multi-layered riprap, will be considered, and their protective effects will be discussed. Based on key scour parameters and riprap layer structural parameters, an empirical model for riprap layer dimensions will be derived to provide theoretical guidance for engineering applications involving riprap layer distribution and thickness.

Author Contributions: B.W.: Investigation; Methodology; Visualization; Writing—original draft. J.L.: Methodology; Writing—review and editing. All authors have read and agreed to the published version of the manuscript.

Funding: This research received no external funding.

Data Availability Statement: The original contributions presented in this study are included in the article. Further inquiries can be directed to the corresponding author.

Acknowledgments: The authors sincerely thank the anonymous reviewers for their valuable suggestions in improving the manuscript.

Conflicts of Interest: The authors declare no conflicts of interest.

References

1. Hao, M.; Li, G.; Sheng, X. Optimizing Pier Arrangement for Flood Hazard Mitigation: A Comparative Mobile-Bed and Fixed-Bed Experimental Study. *Water* **2025**, *17*, 2951. [CrossRef]
2. Ataie-Ashtiani, B.; Beheshti, A.A. Experimental investigation of clear-water local scour at pile groups. *J. Hydraul. Eng.* **2006**, *132*, 1100–1104. [CrossRef]

3. Guo, J.; He, J.X. Dynamic response analysis of ship-bridge collisions experiment. *J. Zhejiang Univ. Sci. A* **2020**, *21*, 525–534. [CrossRef]
4. Bombar, G.; Cardoso, A.H. Effect of Transversal Bed Slope on the Equilibrium Scour Depth at Bridge Piers. *J. Hydraul. Eng.* **2024**, *150*, 04024015. [CrossRef]
5. Wang, X.; Li, W.; Peng, Z.; Yu, Q.; Yang, Y.; Li, J. Optimization of Combined Scour Protection for Bridge Piers Using Computational Fluid Dynamics. *Water* **2025**, *17*, 2742. [CrossRef]
6. Yu, T.S.; Li, Y.C.; Chen, X.G.; Tang, J.H. Experimental study on wave-and current-induced scour around an anti-deposition permeable breakwater. *Ocean Eng.* **2022**, *257*, 111565. [CrossRef]
7. Uzun, Y.; Kumcu, Ş.Y. Prediction of Time Variation of Local Scour Depth at Bridge Abutments: Comparative Analysis of Machine Learning. *Water* **2025**, *17*, 2657. [CrossRef]
8. Pizarro, A.; Manfreda, S.; Tubaldi, E.; Harasti, A.; Gilja, G.; Potočki, K.; Lacko, M. The Science behind Scour at Bridge Foundations: A Review. *Water* **2020**, *12*, 374. [CrossRef]
9. Argyroudis, S.A.; Mitoulis, S.; Winter, M.G.; Kaynia, A.M. Fragility of transport assets exposed to multiple hazards: State-of-the-art review toward infrastructural resilience. *Reliab. Eng. Syst. Saf.* **2019**, *191*, 106567.
10. Richardson, E.V.; Davis, S.R. *Evaluating Scour at Bridges*; Hydraulic Engineering Circular No. 18 (HEC-18), FHWA NHI 01-001; U.S. Federal Highway Administration: Washington, DC, USA, 2001.
11. Zhang, H.; Barrie, A.; Liang, F.; Wang, C. Numerical investigation into the response of a laterally loaded pile in coastal and offshore slopes considering scour effect. *Water* **2025**, *17*, 2032. [CrossRef]
12. Saha, R. A Comprehensive Method of Calculating Maximum Bridge Scour Depth. *Water* **2018**, *10*, 1572. [CrossRef]
13. Omara, H.; Ookawara, S.; Nassar, K.A.; Masria, A.; Tawfik, A. Assessing local scour at rectangular bridge piers. *Ocean Eng.* **2022**, *266*, 112912. [CrossRef]
14. Gazi, A.H.; Purkayastha, S.; Afzal, M.S. The equilibrium scour depth around a pier under the action of Collinear waves and current. *J. Mar. Sci. Eng.* **2020**, *8*, 36. [CrossRef]
15. Sui, T.T.; Liu, C.L.; Zhang, J.S.; Zhang, C.; Zheng, J.H. 3D numerical modeling of wave-monopile-seabed interaction in the presence of a scour hole. *Ocean Eng.* **2024**, *298*, 117254. [CrossRef]
16. Gazi, A.H.; Purkayastha, S.; Afzal, M.S. Scour around Piers under Waves: Current Status of Research and Its Future Prospect. *Water* **2019**, *11*, 2212. [CrossRef]
17. Zhao, P.; Wang, L.; Li, Z.; Zhang, T. Pressure Characteristics of Landslide-Generated Waves on Bridge Piers. *Water* **2023**, *15*, 3623. [CrossRef]
18. Sumer, B.M.; Fredsøe, J.; Christiansen, N. Scour Around Vertical Pile in Waves. *J. Waterw. Port Coast. Ocean Eng.* **1992**, *118*, 15–31. [CrossRef]
19. Liu, J.; Lu, J.; Liang, Z. Computational Simulation of Monopile Scour under Tidal Flow Considering Suspended Energy Dissipation. *Water* **2024**, *16*, 1940. [CrossRef]
20. Kumar, L.; Afzal, M.S. A review of the state of research on bridge pier scour under combined action of waves and current. *Acta Geophys.* **2023**, *71*, 2359–2379. [CrossRef]
21. Moncada-M, A.T.; Aguirre-Pe, J.; Bolívar, J.C.; Flores, E.J. Scour protection of circular bridge piers with collars and slots. *J. Hydraul. Res.* **2009**, *47*, 119–126. [CrossRef]
22. Sumer, B.M.; Dixen, F.H.; Fredsøe, J. Cover stones on liquefiable soil bed under waves. *Coast. Eng.* **2010**, *57*, 864–873. [CrossRef]
23. Zhang, F.P.; Chen, X.G.; Feng, T.; Wang, Y.; Liu, X.X.; Liu, X.L. Experimental study of grouting protection against local scouring of monopile foundations for offshore wind turbines. *Ocean Eng.* **2022**, *258*, 111798. [CrossRef]
24. Melville, B.W.; Hadfield, A.C. Use of sacrificial piles as pier scour countermeasures. *J. Hydraul. Eng.* **1999**, *125*, 1221–1224. [CrossRef]
25. Wang, C.; Liang, F.Y.; Yu, X. Experimental and numerical investigations on the performance of sacrificial piles in reducing local scour around pile groups. *Nat. Hazards* **2017**, *85*, 1417–1435. [CrossRef]
26. Lundkvist, M.; Grue, M.; Friend, P.L.; Flindt, M.R. The relative contributions of physical and microbiological factors to cohesive sediment stability. *Cont. Shelf Res.* **2007**, *27*, 1143–1152. [CrossRef]
27. Tang, Z.H.; Melville, B.; Singhal, N.; Shamseldin, A.; Zheng, J.H.; Guan, D.W.; Cheng, L. Countermeasures for local scour at offshore wind turbine monopile foundations: A review. *Water Sci. Eng.* **2022**, *15*, 15–28. [CrossRef]
28. Khademghaeiny, G.H.; Abrishami, J.; Zarrati, A.R.; Tabarestani, M.K.; Mashahir, M. Riprap design at bridge piers with limited scouring. *Sharif Univ. Technol.* **2020**, *27*, 588–595.
29. Wang, G.; Zhang, Q.; Zhang, J.; Li, X. An experimental study of the local scour protection methods around the monopile foundation of offshore wind turbines. *Ocean Eng.* **2023**, *25*, 41–70. [CrossRef]
30. Guo, J.; Wu, J.Y.; Wang, T. Prediction of local scour depth of sea-crossing bridges based on the energy balance theory. *Ships Offshore Struct.* **2021**, *17*, 2574–2587. [CrossRef]

31. Li, J.; Lian, J.; Guo, Y.; Wang, H.; Yang, X. Numerical study on scour protection effect of monopile foundation based on disturbance structure. *Ocean Eng.* **2022**, *248*, 110856. [CrossRef]
32. Van Rijn, L.C. Sediment transport, part I: Bed load transport. *J. Hydraul. Eng.* **1984**, *110*, 1431–1456. [CrossRef]
33. Daneshfaraz, R.; Ghaderi, A.; Sattariyan, M.; Alinejad, B.; Asl, M.M.; Di Francesco, S. Investigation of local scouring around hydrodynamic and circular pile groups under the influence of river material harvesting pits. *Water* **2021**, *13*, 2192. [CrossRef]
34. Tang, J.H.; Puspasari, A.D. Numerical Simulation of Local Scour around Three Cylindrical Piles in a Tandem Arrangement. *Water* **2021**, *13*, 3623. [CrossRef]
35. Zhang, Y.; Wang, J.F.; Zhou, Q.; Cai, Y.C.; Tang, W. The investigation of local scour around bridge piers with the protection of a quasi-stumps group. *Water* **2023**, *15*, 2858. [CrossRef]
36. Soulsby, R. Chapter 9: Bedload transport. In *Dynamics of Marine Sands*; Thomas Telford Publications: London, UK, 1997.
37. Gippel, C.J.; Bond, N.R.; James, C.; Wang, X. An asset-based, holistic, environmental flows assessment approach. *Int. J. Water Resour. Dev.* **2009**, *25*, 301–330. [CrossRef]
38. Liu, L.; Gu, H.; Yue, P.; Zheng, C.; Zhou, P. Real-time flood forecasting via parameter regionalization and blending nowcasts with NWP Forecasts over the Jiao River, China. *J. Hydrometeorol.* **2023**, *24*, 561–582. [CrossRef]
39. Hou, A.; Tao, J.; Zhu, S. Research on sediment transport process and mechanism change in the Jiaojiang River Estuary, China. *J. Hohai Univ.* **2025**, *53*, 124–134. (In Chinese)
40. Chien, N.; Wan, Z. *Mechanics of Sediment Transport*; ASCE Press: Reston, VA, USA, 2014.
41. Mao, C.X.; Zhou, M.D.; Chai, G.C. *Engineering Hydraulics of Sluice-Dam, Design Management and Research*; China Water Power Press: Beijing, China, 2019. (In Chinese)
42. Zhou, M.D. *Selected Works on Hydraulics of Sluice-Dams for Harnessing the Huaihe River*; China Ocean Press: Beijing, China, 2002. (In Chinese)
43. Mao, C.X.; Zhou, M.D. Local scour on earth bed below sluice-dams. In Proceedings of the 7th Congress APDIAHR, Beijing, China, 13–16 November 1990; Volume 2.
44. *GB 50286-2013*; Code for Design of Project. Beijing China Planning Publishing House: Beijing, China, 2013.
45. Arneson, L.A.; Zevenbergen, L.W.; Lagasse, P.F.; Clopper, P.E. *Evaluating Scour at Bridges*, 5th ed.; U.S. Department of Transportation Federal Highway Administrationm: Washington, DC, USA, 2012.
46. Keulegan, G.H.; Carpenter, L.H. Forces on cylinders and plates in an oscillating fluid. *J. Res. Natl. Bur. Stand.* **1958**, *60*, 423–440. [CrossRef]
47. Richardson, J.; Panchang, V. Three-dimensional simulation of scour-inducing flow at bridge piers. *J. Hydraul. Eng.* **1988**, *124*, 530–540. [CrossRef]
48. Yun, P.; Chen, G. Experimental study on the local scour around the piers of Taizhouwan Bridge. *J. North China Univ. Water Resour. Electr. Power.* **2017**, *38*, 87–92. (In Chinese) [CrossRef]
49. Yang, Y.; Qi, M.; Wang, X.; Li, J. Experimental study of scour around pile groups in steady flows. *Ocean Eng.* **2020**, *195*, 106651. [CrossRef]
50. Yang, Y.; Li, J.; Zou, W.; Chen, B. Numerical Investigation of Flow and Scour around Complex Bridge Piers in Wind–Wave–Current Conditions. *J. Mar. Sci. Eng.* **2024**, *12*, 23. [CrossRef]
51. Yang, Y.L.; Qi, M.L.; Li, J.Z.; Ma, X.D. Evolution of hydrodynamic characteristics with scour hole developing around a pile group. *Water* **2018**, *10*, 1632. [CrossRef]
52. Liang, B.; Du, S.; Pan, X.; Zhang, L. Local scour for vertical piles in steady currents: Review of mechanisms, influencing factors and empirical equations. *J. Mar. Sci. Eng.* **2020**, *8*, 4. [CrossRef]
53. Coleman, S.E. Clearwater local scour at complex piers. *J. Hydraul. Eng.* **2005**, *131*, 330–334. [CrossRef]
54. Zhang, J.S.; Chen, H.; Guo, Y.K.; Wang, F.Y.; Guan, D.W.; Deng, X.; Hou, D.S. Experimental study on the scour characteristics around a jacket foundation under wave actions. *Ocean Eng.* **2024**, *299*, 117290. [CrossRef]
55. Rashno, E.; Zarrati, A.R.; Tabarestani, M.K. Design of riprap for bridge pier groups. *Can. J. Civ. Eng.* **2020**, *47*, 516–522. [CrossRef]
56. Chiew, Y.M. Mechanics of riprap failure at bridge piers. *J. Hydraul. Eng.* **1995**, *121*, 635–643. [CrossRef]
57. Sumer, B.M.; Fredsøe, J. Wave scour around group of vertical piles. *J. Waterw. Port Coast. Ocean Eng.* **1998**, *124*, 248–256. [CrossRef]
58. Liang, S.; Zhang, Y.; Yang, J. An experimental study on pile scour mitigating measures under waves and currents. *Sci. China Technol. Sci.* **2015**, *58*, 85–99. [CrossRef]

Disclaimer/Publisher's Note: The statements, opinions and data contained in all publications are solely those of the individual author(s) and contributor(s) and not of MDPI and/or the editor(s). MDPI and/or the editor(s) disclaim responsibility for any injury to people or property resulting from any ideas, methods, instructions or products referred to in the content.